

THE OXYGEN ABUNDANCE IN THE INNER H II REGIONS OF M101.
IMPLICATIONS FOR THE CALIBRATION OF STRONG-LINE METALLICITY INDICATORS¹

FABIO BRESOLIN

Institute for Astronomy, 2680 Woodlawn Drive, Honolulu, HI 96822; bresolin@ifa.hawaii.edu

ABSTRACT

I present deep spectroscopy of four H II regions in the inner, metal-rich zone of the spiral galaxy M101 obtained with the LRIS spectrograph at the Keck telescope. From the analysis of the collisionally excited lines in two of the target H II regions, H1013 and H493, I have obtained oxygen abundances $12 + \log(\text{O}/\text{H}) = 8.52$ and $12 + \log(\text{O}/\text{H}) = 8.74$, respectively. These measurements extend the determination of the oxygen abundance gradient of M101 via the direct method to only 3 kpc from the center. The intensity of the C II $\lambda 4267$ line in H1013 leads to a carbon abundance $12 + \log(\text{C}/\text{H}) = 8.66$, corresponding to nearly twice the solar value. From a comparison of the continuum temperature derived from the Balmer discontinuity, $T(\text{Bac}) = 5000$ K, and the line temperature derived from [O III] $\lambda 4363/\lambda 5007$, $T[\text{O III}] = 7700$ K, an average temperature $T_0 = 5500$ K and a mean square temperature fluctuation $t^2 = 0.06$ have been derived. Accounting for the spatial inhomogeneity in temperature raises the oxygen abundance obtained from the oxygen auroral lines to $12 + \log(\text{O}/\text{H}) = 8.93$. These findings are discussed in the context of the calibration of strong-line metallicity indicators, in particular of the upper branch of R_{23} . There is no evidence for the strong abundance biases arising from temperature gradients predicted theoretically for metal-rich H II regions.

Subject headings: ISM: abundances — galaxies: ISM — galaxies: abundances — galaxies: individual (M101)

1. INTRODUCTION

As probes of the gas-phase chemical composition of star-forming galaxies, H II regions are crucial targets in the quest to understand the chemical evolution of the Universe. Through the analysis of bright H II regions in external spiral and irregular galaxies it is, in principle, rather straightforward to measure the abundances of elements such as oxygen, nitrogen, neon, argon and sulphur, and therefore constrain models of nucleosynthesis in massive stars and of galactic chemical evolution.

In recent years a great deal of interest has been raised concerning the derivation of chemical abundances in metal-rich H II regions, i.e. those where the oxygen abundance reaches or exceeds that measured in the Sun [$12 + \log(\text{O}/\text{H})_{\odot} = 8.66$, Asplund et al. 2004]². This work is motivated by the importance of obtaining accurate abundances for the measurement and the interpretation of galactic chemical abundance gradients (Pilyugin et al. 2004; Chiappini et al. 2003; Carigi et al. 2005), and for constraining the metal-rich end of the luminosity-metallicity (Kobulnicky & Kewley 2004; Salzer et al. 2005; Maier et al. 2005; Lamareille et al. 2006) and mass-metallicity (Tremonti et al. 2004; Savaglio et al. 2005; Erb et al. 2006) relations of galaxies up to redshifts $z \sim 2$. A large, solar-like oxygen content is inferred for star-forming galaxies both locally (Bresolin et al. 2004; Pilyugin et al. 2006) and at high redshift (Shapley et al. 2004). In addition, empirical metallicity trends in the Wolf-Rayet WC/WN ratio (Meynet & Maeder 2005; Massey 2003) and in the Cepheid Period-Luminosity Relation (Sakai et al. 2004) depend critically on the reliability of the abundances of

metal-rich H II regions.

The difficulty of measuring chemical abundances from the classic analysis of optical forbidden lines (collisionally excited) in high-metallicity H II regions derives from the increased proportion of gas coolants, in particular oxygen, which emits line radiation mostly via the fine-structure [O III] $\lambda\lambda 52,88 \mu\text{m}$ lines. As a consequence of the reduced gas temperature, the auroral-to-nebular line ratios [e.g. [O III] $\lambda 4363/(\lambda 4959 + \lambda 5007)$], employed to determine the electron temperature T_e , become progressively smaller with increasing metallicity, due to the exponential dependence of the collisionally excited line emissivity on T_e . Generally, at metallicities approaching solar the [O III] $\lambda 4363$ auroral line is too faint to be observed in extragalactic nebulae even with 10m-class telescopes, as a result of the strong T_e dependence, and of the fact that the far-IR [O III] lines become stronger at the expense of the optical lines. However, auroral lines from other ionic species can be detected in the optical spectra of H II regions at relatively high abundances, such as [S III] $\lambda 6312$ and [N II] $\lambda 5755$, as a consequence of their larger Boltzmann factors $\exp(-\chi/kT_e)$ (χ is the energy difference, a few eV, between the two levels involved in an auroral line transition). Still, the detection of these diagnostic lines in extragalactic nebulae requires high surface brightness and, generally, 10m-class telescope capabilities.

With the aid of photoionization models (Stasińska 1978; Garnett 1992), one can relate the electron temperature derived for the [S III] or [N II] emitting regions [from [S III] $\lambda 6312/(\lambda 9069 + \lambda 9532)$ and [N II] $\lambda 5755/(\lambda 6548 + \lambda 6583)$, respectively] to the temperature of the [O III] emitting region. When $\lambda 4363$ is unavailable, this allows the measurement of the oxygen abundance from the intensity of the strongest lines only ($\lambda\lambda 4959, 5007$), having fixed the line emissivity from the knowledge of the electron temperature. This technique has been recently applied by Bresolin et al. (2004, 2005) in Keck and VLT studies of the chemical abundances of samples of extragalactic metal-rich H II regions.

¹ The data presented herein were obtained at the W.M. Keck Observatory, which is operated as a scientific partnership among the California Institute of Technology, the University of California and the National Aeronautics and Space Administration. The Observatory was made possible by the generous financial support of the W.M. Keck Foundation.

² The terms *metallicity* and *oxygen abundance* will be used interchangeably throughout the paper. Abundances are measured relative to hydrogen.

The availability of direct abundances is essential for the empirical calibration of the so-called *strong-line methods*, in which the strength of easily observed nebular emission lines are related to the metallicity of the emitting regions. Among the various methods proposed, I recall $R_{23} = ([\text{O II}] \lambda 3727 + [\text{O III}] \lambda \lambda 4959, 5007) / \text{H}\beta$ (Pagel et al. 1979), $N_2 = [\text{N II}] \lambda 6583 / \text{H}\alpha$ (Storchi-Bergmann et al. 1994; Denicoló et al. 2002), $\text{O3N2} = ([\text{O III}] \lambda 5007 / \text{H}\beta) / ([\text{N II}] \lambda 6583 / \text{H}\alpha)$ (Alloin et al. 1979; Pettini & Pagel 2004), $S_{23} = ([\text{S II}] \lambda \lambda 6717, 6731 + [\text{S III}] \lambda \lambda 9069, 9532) / \text{H}\beta$ (Vílchez & Esteban 1996; Díaz & Pérez-Montero 2000), the P-method (Pilyugin 2000; Pilyugin & Thuan 2005) and $\text{Ar}_3\text{O}_3 = [\text{Ar III}] \lambda 7135 / [\text{O III}] \lambda 5007$, $\text{S}_3\text{O}_3 = [\text{S III}] \lambda 9069 / [\text{O III}] \lambda 5007$ (Stasińska 2006). For in-depth discussions of these abundance indicators the reader is referred to these papers, as well as to Kewley & Dopita (2002), Pérez-Montero & Díaz (2005) and Dopita et al. (2006a). The strong-line methods allow the estimation of nebular chemical abundances in cases where a direct approach, based on the detection of the auroral lines, is not feasible, and in general when the signal-to-noise ratio of the spectra is sufficient to measure only a restricted number of emission lines. This approach is widely adopted for the determination of abundance gradients in galaxies (Pilyugin et al. 2004, 2006) and of oxygen abundances in intermediate- and high-redshift star-forming galaxies (Shapley et al. 2004; Savaglio et al. 2005; Mouhcine et al. 2006). The popularity of these metallicity indicators is also due to the increasing necessity of estimating chemical abundances for galaxies observed as part of large spectroscopic surveys, such as the Sloan Digital Sky Survey (Tremonti et al. 2004; Liang et al. 2006; Shi et al. 2006).

Calibrations of strong-line methods based on grids of photoionization models (e.g. Edmunds & Pagel 1984; McGaugh 1991; Zaritsky et al. 1994; Charlot & Longhetti 2001; Kewley & Dopita 2002) provide abundances that are, at the metal-rich end, considerably larger (up to 0.5 dex) than those obtained from direct measurements (Castellanos et al. 2002; Kennicutt et al. 2003; Garnett et al. 2004b; Bresolin et al. 2004, 2005) or from T_e -calibrated empirical methods. Mixing T_e -based abundances (routinely done at low metallicity) with abundances from model grids (at large metallicity) leads then to spurious discontinuities in abundance diagnostic diagrams or breaks in the luminosity-metallicity relation (Nagao et al. 2006; Lee et al. 2006). The reasons for the discrepancy are still currently poorly known: additional sources of heating need to be postulated in order to reproduce theoretically the measured $[\text{O III}] \lambda 4363$ line strength (Stasińska & Schaerer 1999; Luridiana et al. 1999).

There are a number of open issues regarding the study of metal-rich H II regions that motivate further investigation of ionized nebulae in nearby galaxies. First of all is the assessment of the importance of the effects of temperature gradients in H II regions and the resulting abundance biases, expected from theoretical models (Stasińska 1980). As the metallicity approaches the solar value, strong temperature gradients develop in H II regions, due to the more efficient cooling in the central zone from far-IR $[\text{O III}]$ fine-structure lines relative to the outer region. Since the line strength is weighed towards warmer regions, due to the strong T_e dependence of the line emissivities, the net effect of these temperature gradients is that the electron temperature derived from the auroral lines over-estimates the real temperature, and consequently the

oxygen abundance is systematically under-estimated (Garnett 1992; Stasińska 2005). In general, in the presence of spatial temperature variations within H II regions, methods based on collisionally excited lines can lead to under-estimate chemical abundances by a factor of two or more (Peimbert 1967; Torres-Peimbert et al. 1980).

Alternative methods of abundance determination, less dependent on the nebular temperature structure than collisionally excited lines, need therefore to be explored in extragalactic H II regions of high metal content. Metal recombination lines and infrared fine-structure lines offer such alternatives. In both cases the line emissivity is only moderately dependent on T_e . There are obvious difficulties in exploiting these techniques, however: recombination lines are very weak and hard to detect in extragalactic H II regions (Esteban et al. 2002), and infrared observations require orbiting telescopes (Garnett et al. 2004a).

Studies of the O II recombination lines in Galactic and extragalactic H II regions find oxygen abundances 2 to 3 times larger than those obtained from $[\text{O III}] \lambda 4363 / (\lambda 4959 + \lambda 5007)$, and conclude that the discrepancy can be explained by the presence of temperature fluctuations (Peimbert et al. 1993; Peimbert 2003; García-Rojas et al. 2006). There is still no general consensus about the source of temperature fluctuations in H II regions and planetary nebulae (Peimbert & Peimbert 2006), and alternative explanations for the abundance discrepancy between collisionally excited lines and recombination lines have been proposed (Liu et al. 2000; Tsamis & Péquignot 2005).

In this paper I report on new deep spectroscopic observations of four H II regions in the inner zone of the spiral galaxy M101. The radial oxygen abundance gradient in this galaxy has been studied in detail by previous authors (Torres-Peimbert et al. 1989; Kennicutt et al. 2003, hereafter KBG03). The oxygen abundance of the innermost H II regions studied thus far, using auroral line detections, is approximately $12 + \log(\text{O}/\text{H}) = 8.7$, with an extrapolated central abundance $12 + \log(\text{O}/\text{H}) = 8.76$ (KBG03), corresponding to $1.26(\text{O}/\text{H})_{\odot}$. The new observations presented in this paper provide additional high-quality spectroscopic data for some of the most metal-rich H II regions in this galaxy, with the goals of: (a) obtaining direct abundances closer to the galaxy nucleus from auroral lines; (b) verifying, if feasible, these abundances using metal recombination lines, and (c) measure the effects of temperature fluctuations on the direct abundances. Observations and data reduction are explained in §2. The abundances derived from collisionally excited lines in two H II regions are presented in §3, while those derived from recombination lines for helium and carbon for one of them are presented in §4 and §5, respectively. A measure of the temperature fluctuations in one of these H II regions, and their effect on the chemical abundances derived from collisionally excited lines, is given in §6. In §7 I discuss the implications of the results obtained for the calibration of strong-line metallicity indicators. The main results of this paper are summarized in §8.

2. OBSERVATIONS

The four targets chosen for this investigation are among the brightest H II regions in the central 3 arcminutes (~ 6 kpc at a distance of 6.85 Mpc, Freedman et al. 2001) of M101: H493, H507 (also Searle 2, from Searle 1971), H972 and H1013 (Searle 3). Table 1 contains the identification and the celestial coordinates taken from the catalog of Hodge et al.

(1990), together with the deprojected galactocentric distance in units of the disk isophotal radius ($R_0 = 14.4$), taken from Kennicutt & Garnett (1996).

The spectra of the H II regions were obtained on May 12, 2005 with the Keck I telescope on Mauna Kea using the Low Resolution Imaging Spectrometer (Oke et al. 1995). The observing conditions were photometric, and the seeing was stable at $0.7''$ throughout the night. Using a dichroic splitter, blue and red spectra were obtained simultaneously over most of the optical wavelength range. For the blue spectra (3300-5600 Å) a 600 lines mm^{-1} grism blazed at 4000 Å was employed, yielding a spectral resolution of ~ 5 Å with a 1.5 arcsec-wide slit. In the red (4960-6670 Å) a 900 lines mm^{-1} grating blazed at 5500 Å was used (4 Å resolution). In order to extend the spectral coverage to the near-infrared [S III] lines, spectra were obtained also with a 400 lines mm^{-1} grating blazed at 8900 Å, covering the 6050-9800 Å wavelength range at 9 Å resolution.

The total integration time for the blue and red spectra ranged between 4200 and 4500 seconds, split into two or three exposures. For the near-IR spectra single 300 s or 900 s exposures were obtained. I also acquired 300 s blue and red spectra for the two brightest nebulae, H1013 and H972, in order to avoid saturation of the $H\alpha$ emission line. Table 1 summarizes the exposures secured for this program.

The airmass of M101 varied during the observations between 1.21 and 1.83. In order to minimize the effects of differential atmospheric refraction the position angle of the slit was adjusted to match the parallactic angle as it varied during the course of the night. Observations of the standard stars LTT 7987, BD+28d4211 and BD+25d4655 were obtained during twilight for flux calibration.

2.1. Data reduction and line flux measurement

The long-slit data reduction was carried out with IRAF³, version 2.12, using the PYRAF⁴ command language. The spectra were corrected for bias, flat-fielded and wavelength calibrated using Hg + Zn + Cd lamps (blue range) and Ne + Ar lamps (red range). For the flux calibration the Mauna Kea extinction curve of Krisciunas et al. (1987) was employed. Due to the lack of proper calibration data, the flux calibration at wavelengths longer than 9200 Å was not carried out. Spectral regions in common between adjacent wavelength ranges showed a good agreement in the calibrated continuum level and in the flux of lines in common, indicating a 5% accuracy in the relative flux calibration.

The strength of the emission lines was measured by integration of the flux under the line profile, measured between two continuum points selected interactively. These fluxes were corrected for interstellar reddening adopting the Howarth (1983) analytical formulation of the Seaton (1979) law. The reddening coefficient $C(H\beta)$ was obtained from the Balmer decrement, considering the measured intensities of $H\alpha$ and $H\gamma$ relative to $H\beta$, compared to the case B values taken from Storey & Hummer (1995) for an electron temperature $T_e = 7500$ K. The equivalent width of the Balmer lines in absorption originating from the underlying stellar compo-

nent was adjusted iteratively in order to reach agreement in the $C(H\beta)$ determined separately from the $H\alpha/H\beta$ and $H\gamma/H\beta$ ratios. Higher order lines of the Balmer series are progressively more sensitive to the amount of underlying absorption, and were thus not included in this procedure.

The result of the line flux measurements, corrected for reddening, is presented in Table 2. The quoted uncertainties account for statistical errors, as well as the uncertainty in the flux calibration, the flat-fielding, and the reddening. I have compared the fluxes of the strongest metal lines with the values published by Kennicutt & Garnett (1996). In general there is agreement at the 1- σ level. The comparison is slightly worse (2- σ) for the [O II] $\lambda 3727$ line in H1013 and H507. In similar comparisons (e.g. Bresolin et al. 2005) the [O II] $\lambda 3727$ is often found to be the one showing the largest discrepancy. It is not clear if this is due simply to errors in the line flux measurements and/or reddening corrections, or if variations in the regions sampled by the various slits can also account for the observed differences.

As Table 2 shows, auroral lines have been detected in three of the four targets: H493, H507 and H1013. These lines will be used in Section 3 to derive electron temperatures and ionic abundances from the collisionally excited lines. The [N II] $\lambda 5755$, [S III] $\lambda 6312$ and [O II] $\lambda 7325$ auroral lines have already been measured in H1013 by KBG03. For these lines the comparison with the fluxes presented here is excellent.

The spectrum of H507 shows a large number of Fe II lines (Fig. 1), resembling the emission-line rich spectra of known luminous Galactic iron stars, such as HD 316285 and η Carinae (Walborn & Fitzpatrick 2000). These are massive stars believed to be in an advanced stage of evolution. The presence of evolved massive stars in H507 is also evident from the Wolf-Rayet emission features at ~ 4650 Å (both the N III $\lambda\lambda 4634-42$ and the He II $\lambda 4686$ are detected, indicative of WN stars) and 5696 Å from C III (late WC stars). In fact, W-R emission lines have been detected in all four H II regions studied here. The high detection fraction of W-R features, often including the signatures of WC stars, in high-metallicity H II regions has been noted in earlier works (Bresolin et al. 2004, 2005; Hadfield et al. 2005), and is expected from the increase in the stellar mass loss with metallicity (Meynet & Maeder 2005). Given the scope of this paper, I will not further discuss the W-R content of the H II regions under consideration, and I will simply note that the stellar envelope of stars with Fe II lines in emission can also be responsible for emission in auroral lines such as [N II] $\lambda 5755$ and [O II] $\lambda 7325$ (Hillier et al. 1998, Borges Fernandes et al. 2001). Therefore, these lines will not be used to measure nebular electron temperatures in H507.

Electron densities were estimated from the [S II] $\lambda 6716/\lambda 6731$ line ratio, which in all H II regions is consistent with the low-density limit. This is also the case for the [Cl III] $\lambda 5518/\lambda 5538$ ratio measured for H1013, compared to the theoretical low-density value (Keenan et al. 2000). A common density $N_e = 100 \text{ cm}^{-2}$ will therefore be adopted in the remainder of the paper for all H II regions.

3. METAL ABUNDANCES FROM COLLISIONALLY EXCITED LINES

The following analysis focuses on the two H II regions for which reliable electron temperatures could be measured: H493 and H1013. For the derivation of ionic abundances from collisionally excited lines I relied on the programs by Shaw & Dufour (1995) available in the STSDAS *nebular* package running under IRAF. The atomic parameters and the col-

³ IRAF is distributed by the National Optical Astronomy Observatories, which are operated by the Association of Universities for Research in Astronomy, Inc., under cooperative agreement with the National Science Foundation.

⁴ PYRAF is a product of the Space Telescope Science Institute, which is operated by AURA for NASA.

TABLE 1
OBJECT SAMPLE AND EXPOSURES ACQUIRED

Object	R.A. (J2000.0)	DEC. (J2000.0)	R/R_0	3300-5600 Å	Exposures 4960-6670 Å	6050-9800 Å
H493.....	14:03:03.4	+54:21:25	0.10	3×1500 s	3×1500 s	1×900 s
H507 (Searle 2).....	14:03:04.2	+54:19:28	0.14	3×1500 s	3×1500 s	1×900 s
H972.....	14:03:27.8	+54:21:31	0.16	2×2100 s 1×300 s	2×2100 s 1×300 s	1×300 s
H1013 (Searle 3)....	14:03:30.7	+54:21:14	0.19	3×1500 s 1×300 s	3×1500 s 1×300 s	1×300 s

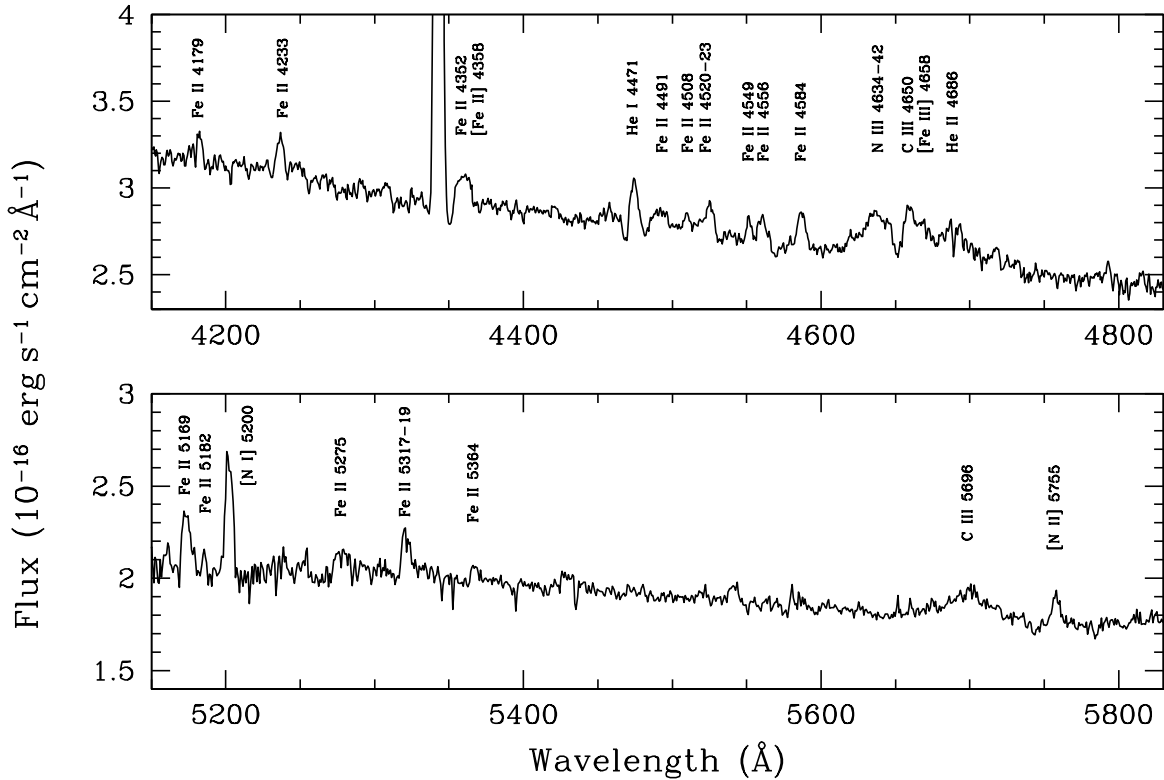


FIG. 1.— The spectrum of H507 contains a large number of Fe II lines, some are shown here in the 4150-4830 Å (top) and 5150-5830 Å (bottom) wavelength ranges. The Wolf-Rayet features at ~ 4650 Å and 5696 Å are also labeled.

lision strengths adopted are those implemented in the 1997 version of the software, except for the S III collision strengths, which were taken from Tayal & Gupta (1999).

In the case of H1013 five values of the electron temperature were derived from the ratios of the available auroral lines to the corresponding nebular lines (see Table 3). The values from the different ions are all similar to each other, and are in the 7680–8360 K range. The ionic abundances were derived adopting $T[\text{O III}]$ for O^{++} and Ne^{++} , $T[\text{S III}]$ for S^{++} and Ar^{++} , $T[\text{S II}]$ for S^+ , and a weighted average of $T[\text{O II}]$ and $T[\text{N II}]$, corresponding to 8070 ± 120 K, for O^+ and N^+ .

For H493 only $T[\text{S III}]$ and $T[\text{N II}]$ could be directly measured. In this case, therefore, I determined the temperature relative to the O^{++} emission zone (assumed to be equal to the temperature measured from the $[\text{O III}]$ lines) following previous papers in this series (Bresolin et al. 2004, 2005), i.e. by adopting the relationship between $T[\text{O III}]$ and $T[\text{S III}]$ predicted by photoionization models (Garnett 1992, Stasińska

1982):

$$T[\text{S III}] = 0.83 T[\text{O III}] + 1700 \text{ K} \quad (1)$$

where the electron temperatures are in K. However, because oxygen is present in H493 almost exclusively as O^+ , this procedure has a very little impact on the derived total oxygen abundance. The other assumption made in the abundance analysis of H493 is that $T[\text{N II}]$ can be used for the determination of ionic abundances of all the low-ionization species.

From the electron temperatures in Table 3 the ionic abundances presented in Table 4 were derived. To calculate the total abundances of oxygen, nitrogen and sulfur, the following equations were used:

$$\text{O}/\text{H} = (\text{O}^+ + \text{O}^{++})/\text{H}^+ \quad (2)$$

$$\text{N}/\text{O} = \text{N}^+/\text{O}^+ \quad (3)$$

TABLE 2
REDDENING-CORRECTED LINE FLUXES

Line		H493	H507	H972	H1013
3727	[O II]	84 ± 4	84 ± 4	139 ± 7	221 ± 11
3750	H 12	...	1.8 ± 0.2	...	3.0 ± 0.2
3771	H 11	...	4.7 ± 0.3	...	3.3 ± 0.2
3798	H 10	6.3 ± 0.3	5.3 ± 0.3	...	4.4 ± 0.2
3822	He I	0.72 ± 0.06
3835	H 9	8.3 ± 0.4	7.1 ± 0.4	...	7.3 ± 0.3
3868	[Ne III]	3.1 ± 0.2
3969	H 8	16.0 ± 0.7	12.5 ± 0.6	18.1 ± 0.7	16.4 ± 0.7
4026	He I	1.54 ± 0.08
4072 †	[S II]	1.27 ± 0.07
4101	Hδ	26.4 ± 1.1	26.4 ± 1.1	27.5 ± 1.1	26.2 ± 1.1
4144	He I	0.13 ± 0.03
4267	C II	0.25 ± 0.03
4340	Hγ	46.3 ± 1.8	46.4 ± 1.9	46.4 ± 1.7	46.4 ± 1.9
4363 †	[O III]	0.24 ± 0.03
4388	He I	0.40 ± 0.05
4471	He I	1.2 ± 0.2	2.2 ± 0.2	1.2 ± 0.1	3.9 ± 0.2
4658	[Fe III]	0.40 ± 0.05
4711	[Ar IV]	0.35 ± 0.04
4861	Hβ	100 ± 4	100 ± 4	100 ± 4	100 ± 4
4922	He I	...	1.46 ± 0.15	...	1.02 ± 0.05
4959	[O III]	3 ± 0	2 ± 0	9 ± 0	33 ± 1
4986	[Fe III]	...	0.31 ± 0.14	...	0.35 ± 0.04
5007	[O III]	8 ± 0	8 ± 0	30 ± 1	102 ± 4
5016	He I	0.90 ± 0.10	2.87 ± 0.20	1.16 ± 0.15	2.44 ± 0.10
5041	Si II	0.17 ± 0.02
5048	He I	0.13 ± 0.02
5056	Si II	0.55 ± 0.10	0.17 ± 0.02
5199	[N I]	1.43 ± 0.13	3.17 ± 0.20	0.84 ± 0.13	0.62 ± 0.03
5270	[Fe III]	0.15 ± 0.02
5518	[Cl III]	0.46 ± 0.03
5538	[Cl III]	0.29 ± 0.02
5755 †	[N II]	0.24 ± 0.06	0.51 ± 0.12	...	0.59 ± 0.03
5876	He I	6.7 ± 0.3	6.9 ± 0.3	8.5 ± 0.4	12.1 ± 0.6
5978	Si II	0.13 ± 0.02
6046	[O I]	0.09 ± 0.02
6300	[O I]	1.17 ± 0.10	1.84 ± 0.11	...	1.21 ± 0.07
6312 †	[S III]	0.27 ± 0.07	0.77 ± 0.05
6360	[O I]	0.37 ± 0.06	0.60 ± 0.06	...	0.30 ± 0.03
6548	[N II]	32 ± 2	30 ± 2	27 ± 1	24 ± 1
6563	Hα	294 ± 15	294 ± 16	293 ± 15	293 ± 16
6583	[N II]	95 ± 5	88 ± 5	80 ± 4	71 ± 4
6678	He I	2.2 ± 0.2	2.3 ± 0.2	2.3 ± 0.2	3.4 ± 0.2
6717	[S II]	30.2 ± 1.7	30.1 ± 1.7	24.1 ± 1.3	17.8 ± 1.0
6731	[S II]	21.2 ± 1.2	22.0 ± 1.2	16.9 ± 0.9	12.0 ± 0.7
7065	He I	...	1.49 ± 0.19	1.41 ± 0.18	1.81 ± 0.11
7135	[Ar III]	1.5 ± 0.2	1.3 ± 0.1	3.8 ± 0.3	7.1 ± 0.4
7236	C II	...	1.02 ± 0.18	...	0.27 ± 0.03
7281	He I	0.51 ± 0.05
7325 †	[O II]	...	0.9 ± 0.2	...	2.4 ± 0.2
7751	[Ar III]	1.54 ± 0.11
8545	P 15	0.69 ± 0.06
8598	P 14	0.66 ± 0.07
8665	P 13	0.82 ± 0.09
8750	P 12	1.07 ± 0.11
8863	P 11	...	1.14 ± 0.13	...	1.35 ± 0.12
9015	P 10	1.51 ± 0.24	1.39 ± 0.15	...	1.86 ± 0.15
9069	[S III]	10 ± 2	9 ± 2	17 ± 3	24 ± 5
C(Hβ)		0.48 ± 0.05	0.74 ± 0.05	0.40 ± 0.05	0.35 ± 0.05
EW(Hβ)		59 ± 1	48 ± 1	34 ± 1	146 ± 1
F(Hβ) ^a		29.0 ± 1	63.4 ± 1	31.8 ± 1	157.0 ± 1

NOTE. — Some lines belonging to a doublet/multiplet are identified by a single wavelength, for example [O II] λλ3726, 3729 (here [O II] λ3727), [S II] λλ4069, 4076 ([S II] λ4072) and [O II] λλ7319, 7320 + λλ7329, 7330 ([O II] λ7325). Auroral lines are identified by the † symbol.

^aExtinction-corrected total flux, in units of 10^{-15} erg s⁻¹ cm⁻².

TABLE 3
MEASURED ELECTRON TEMPERATURES (K)

	auroral nebular	H493	H1013
T[O III].....	$\frac{4363}{4959+5007}$...	7700 ± 250
T[O II].....	$\frac{7325}{3727}$...	7690 ± 200
T[N II].....	$\frac{5755}{6548+6583}$	5960 ± 340	8360 ± 150
T[S II].....	$\frac{4072}{6717+6731}$...	8160 ± 340
T[S III].....	$\frac{6312}{9069+9532}$	7330 ± 590	7680 ± 160

TABLE 4
IONIC AND TOTAL ABUNDANCES FROM
COLLISIONALLY EXCITED LINES

	H493	H1013
O^+/H^+	$5.4 \pm 2.3 \times 10^{-4}$	$2.3 \pm 0.2 \times 10^{-4}$
O^{++}/H^+	$1.4 \pm 0.8 \times 10^{-5}$	$9.9 \pm 1.4 \times 10^{-5}$
N^+/H^+	$1.0 \pm 0.2 \times 10^{-4}$	$2.6 \pm 0.1 \times 10^{-5}$
S^+/H^+	$6.1 \pm 1.4 \times 10^{-6}$	$1.2 \pm 0.1 \times 10^{-6}$
S^{++}/H^+	$3.1 \pm 0.7 \times 10^{-6}$	$6.7 \pm 0.3 \times 10^{-6}$
Ar^{++}/H^+	$3.3 \pm 0.8 \times 10^{-7}$	$1.3 \pm 0.1 \times 10^{-6}$
Ne^{++}/H^+	$1.1 \pm 0.2 \times 10^{-5}$
$12 + \log(O/H)$..	8.74 ± 0.17	8.52 ± 0.05
$\log(N/O)$	-0.72 ± 0.22	-0.95 ± 0.05
$\log(S/O)$	-1.78 ± 0.20	-1.61 ± 0.05

as suggested by Peimbert & Costero (1969), and

$$\frac{S^+ + S^{++}}{S} = \left[1 - \left(1 - \frac{O^+}{O} \right)^\alpha \right]^{1/\alpha}, \quad (4)$$

following Stasińska (1978) with $\alpha = 2.5$. This last equation yields very small corrections ($\sim 1\%$ or less) to the sulfur abundance in both H493 and H1013, due to the low amount of S^{3+} expected in low-excitation nebulae (see also KBG03, Bresolin et al. 2004). The O/H, N/O and S/O abundance ratios thus derived are included in Table 4.

KBG03 determined the oxygen abundance gradient in M101 from 20 H II regions in which the electron temperature of the gas could be determined from ratios of auroral lines to nebular lines. The galactocentric distances of these H II regions vary between $R/R_0 = 0.19$ (H1013) and $R/R_0 = 1.25$ (SDH323). The new measurements presented here add one further point closer to the center of the galaxy, H493 at $R/R_0 = 0.10$, and allow a determination of the O^{++} abundance of H1013 from a direct measurement of [O III] $\lambda 4363$. The resulting O/H abundance is ~ 0.2 dex lower than measured by KBG03: $12 + \log(O/H) = 8.52 \pm 0.06$ (this work) vs. $12 + \log(O/H) = 8.71 \pm 0.05$ (KBG03). The differences in the adopted O^+ temperature (8070 K vs. 7600 K) and in the O^{++} temperature (7700 K vs. 6600 K) are responsible, in approximately equal proportions, for the discrepancy in abundance. The O^{++} zone temperature was derived by KBG03 from $T[S III]$, measured from the [S III] $\lambda 6312/(\lambda 9069 + \lambda 9532)$ line ratio, and the application of Equation (1). The $T[S III]$ value determined in the current work is ~ 500 K higher than the

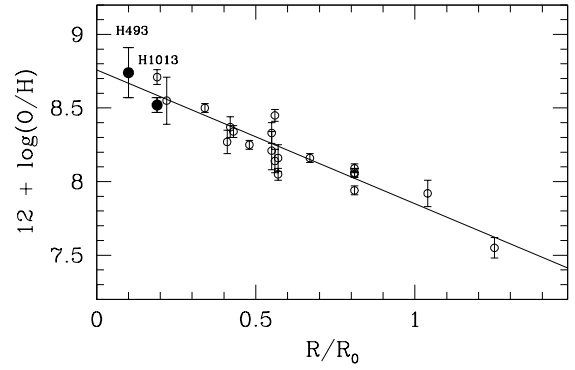


FIG. 2.— The oxygen abundance gradient in M101 in terms of the fractional isophotal radius, R/R_0 , determined from the KBG03 measurements (open circles) and the inner regions H493 and H1013 studied here (full dots). All the data points represent H II regions where the electron temperature has been measured directly from auroral-to-nebular line ratios. In all cases, except for the innermost region, H493, and H336 (= Searle 5, point at $R/R_0 = 0.22$) the [O III] temperature has been derived from the $\lambda 4363$ line. In this plot the straight line represents the weighted linear least square fit, given by Eq. (5).

KBG03 value, as a result of a $\sim 35\%$ smaller flux in the [S III] $\lambda \lambda 9069, 9532$ lines. I point out that Equation (1), together with the value of $T[S III]$ in Table 3, would provide $T[O III] = 7200 \pm 200$ K, i.e. 500 K smaller than measured directly from [O III] $\lambda 4363/(\lambda 4959 + \lambda 5007)$. The relation proposed by Pérez-Montero & Díaz (2005), $T[S III] = 1.05 T[O III] - 800$ K, would yield instead $T[O III] = 8100 \pm 150$ K. This result is a warning that relations derived from photoionization models, such as Equation (1), can work well in a statistical sense, but can fail for individual H II regions when uncertainties in T_e smaller than a few hundred degrees are required.

A weighted linear least square fit to the KBG03 data points, supplemented by the abundances determined here for H493 and H1013, provides the following solution for the radial oxygen abundance gradient in M101:

$$12 + \log(O/H) = 8.75 (\pm 0.05) - 0.90 (\pm 0.07) R/R_0. \quad (5)$$

This relation is virtually the same as the one determined by KBG03. The innermost region studied in this paper, H493, allows us to extend the empirical abundance gradient in M101 to 1.5 arcmin from the galactic center. The oxygen abundance of H493, $12 + \log(O/H) = 8.74 \pm 0.17$, agrees well with the galactic abundance gradient, as shown in Fig. 2.

4. HELIUM ABUNDANCES

There are several He I recombination lines which could, in principle, be used to obtain the helium abundance, especially in the case of H1013 (see Table 2). However, many of these lines are faint, with small equivalent widths, and the abundances derived from them would be quite sensitive to even small corrections for underlying absorption. Some of the stronger lines are not well suited for the measurement of the helium abundance either, because they are partially blended with strong metal lines, as in the case of He I $\lambda 5016$ with [O III] $\lambda 5007$, or they can be strongly affected by optical depth effects (He I $\lambda 7065$). Therefore, only the two lines He I $\lambda 5876$ and $\lambda 6678$ have been used.

The He^+/H^+ ionic ratios have been obtained from He I $\lambda 5876/H\beta$ and He I $\lambda 6678/H\beta$, adopting the emissivities of Benjamin et al. (1999) for He I and of Storey & Hummer

TABLE 5
IONIC AND TOTAL ABUNDANCES FROM
RECOMBINATION LINES

	H493	H1013
He ⁺ /H ⁺	0.048 ± 0.003	0.083 ± 0.001
He/H	0.10 ± 0.01	0.10 ± 0.01
C ⁺⁺ /H ⁺	2.3 ± 0.3 × 10 ⁻⁴
12 + log(C ⁺⁺ /H ⁺)	...	8.36 ± 0.06
12 + log(C/H)	...	8.66 ± 0.07

(1995) for H I, both calculated at the $T[\text{O III}]$ temperature determined in the previous section. The average ionic abundances thus derived from $\lambda 5876$ and $\lambda 6678$ are reported in Table 5. In the case of the low excitation H II region H493 I find $\text{He}^+/\text{H}^+ = 0.048$, almost half the value found in H1013, $\text{He}^+/\text{H}^+ = 0.083$. These helium ionic fractions should be compared to oxygen ionic fractions $\text{O}^+ / (\text{O}^+ + \text{O}^{++})$ of 0.97 (H493) and 0.70 (H1013; a value of 0.55 is however derived when accounting for the presence of temperature fluctuations, as shown in § 6).

A large fraction of the helium present in low-excitation nebulae is in the neutral form. To estimate its contribution to the total helium abundance, a grid of photoionization models has been obtained with CLOUDY 94.00 (Ferland et al. 1998). The helium ionization correction factor, ICF(He), has been estimated from the predicted relation between $\text{He}^0 / (\text{He}^0 + \text{He}^+)$ and $\text{O}^+ / (\text{O}^+ + \text{O}^{++})$ (He^{++} is negligible at these low excitation levels). I found $\text{ICF}(\text{He}) = 2.13 \pm 0.23$ for H493 and $\text{ICF}(\text{He}) = 1.28 \pm 0.09$ for H1013 (1.20 ± 0.09 accounting for temperature fluctuations). The resulting helium abundances for H493 ($\text{He}/\text{H} = 0.10 \pm 0.01$) and H1013 [$\text{He}/\text{H} = 0.11 \pm 0.01$, or $\text{He}/\text{H} = 0.10 \pm 0.01$ if using $\text{O}^+ / (\text{O}^+ + \text{O}^{++}) = 0.55$] are in agreement, within the uncertainties.

5. THE CARBON ABUNDANCE OF H1013

The C II $\lambda 4267$ recombination line has been detected in H1013, the brightest of the H II regions studied in this work (Fig. 3). Esteban et al. (2002) measured this line, as well as various O II lines, in two H II regions of lower metallicity in M101, NGC 5471 and NGC 5461. Metal recombination lines allow the determination of ionic abundances that are virtually independent of the electron temperature, thanks to the fact that they have a similar temperature dependence as the hydrogen recombination lines, and therefore allow very important checks on the abundances obtained from collisionally excited lines. Unfortunately, no O II lines could be measured in the LRIS spectra. This is likely a result of the low spectral resolution, combined with the fact that the strongest oxygen recombination lines around 4650 Å fall in the spectral region occupied by the strong W-R blue bump. Besides, at the low excitation levels typical of the H II regions considered here, most of the oxygen is in the O^+ form rather than O^{++} , as shown in the previous section. As a consequence, the O II recombination lines will be very faint. This problem affects most metal-rich H II regions, which are generally of low excitation (see Sect. 7).

Because of the lack of collisionally excited lines from carbon in the optical spectra of H II regions, and the current unavailability of UV spectrographs working in space for the study of lines like C III] $\lambda 1909$, the derivation of the C^{++}/H^+

ratio and of the total C/H abundance in extragalactic nebulae from the detection of recombination lines is very important to study the chemical evolution of spiral galaxies. In the case of the center of M101, it is interesting to test whether the C II $\lambda 4267$ recombination line provides a carbon abundance that is consistent with the measured oxygen abundance. For this purpose, I have adopted the C II effective recombination coefficient $\alpha_{\text{C II}}$ from Davey et al. (2000) and used the following expression to derive the abundance of C^{++} :

$$\frac{\text{C}^{++}}{\text{H}^+} = \frac{I(4267)}{I(\text{H}\beta)} \frac{4267}{4861} \frac{\alpha_{\text{H}\beta}}{\alpha_{\text{C II}}} \quad (6)$$

where the $\text{H}\beta$ effective recombination coefficient $\alpha_{\text{H}\beta}$ has been obtained from the Storey & Hummer (1995) emissivities. Both α 's have been calculated at the $T[\text{O III}]$ temperature. The resulting ionic abundance fraction is $\text{C}^{++}/\text{H}^+ = 2.3 \times 10^{-4}$, equivalent to $12 + \log(\text{C}^{++}/\text{H}^+) = 8.36 \pm 0.06$ (Table 5).

In order to account for the C^+ contribution to the total C abundance (C^{3+} is negligible in the low-excitation regime), a procedure similar to the one adopted for the helium ICF has been followed, i.e. the C^+/C fraction as a function of O^+/O predicted by photoionization models was considered. The result $\text{C}^+/\text{C} = 0.61 \pm 0.02$ has been obtained. The models by Garnett et al. (1999) would yield the same result. Adopting instead $\text{O}^+/\text{O} = 0.55$, as determined in § 6, I obtain instead $\text{C}^+/\text{C} = 0.50 \pm 0.02$. The latter value is adopted, to infer a total carbon abundance for H1013 of $12 + \log(\text{C}/\text{H}) = 8.66 \pm 0.06$. This value corresponds to 1.9 times the solar value (Asplund et al. 2005). Fig. 4 compares the O/H and C/O abundance determined for H1013 with data from the literature. Abundances obtained from collisionally excited lines (H II regions in spiral and irregular galaxies from Garnett et al. 1995, 1997, 1999; Kobulnicky & Skillman 1998) and from recombination lines (H II regions in the Milky Way and other spirals, Esteban et al. 2002, 2005; Peimbert 2003; Peimbert et al. 2005) are shown. The H1013 datapoint should be compared with the latter set only, but the collisionally excited line results are also included for completeness (the dotted lines connect H II regions in common between the two sets: NGC 5461 and NGC 5471 in M101, and 30 Doradus in the LMC).

6. TEMPERATURE FLUCTUATIONS IN H1013

Thanks to the excellent blue sensitivity of LRIS, the Balmer discontinuity at 3646 Å is very well observed in the nebular spectra presented in this work (the case of H1013 can be seen in the top panel of Fig. 3). The nebular Balmer jump offers the opportunity to derive an electron temperature that is independent of the collisionally excited lines of metals, and representative of the hydrogen continuum spectrum, $T(\text{Bac})$. As shown originally by Peimbert (1967) and Peimbert & Costero (1969), the comparison between two independently derived temperatures, e.g. $T(\text{Bac})$ and $T[\text{O III}]$, provides an indication about the presence of temperature fluctuations in H II regions and planetary nebulae. In the following I analyze the H II region H1013, where the contribution to the nebular continuum by underlying stars (direct and scattered) appears to be negligible, as judged by the small equivalent width (0.1 Å) of the Balmer lines in absorption inferred during the reddening correction. I follow the technique developed by Peimbert & Costero (1969) and summarized in several recent papers, for example by Peimbert et al. (2004).

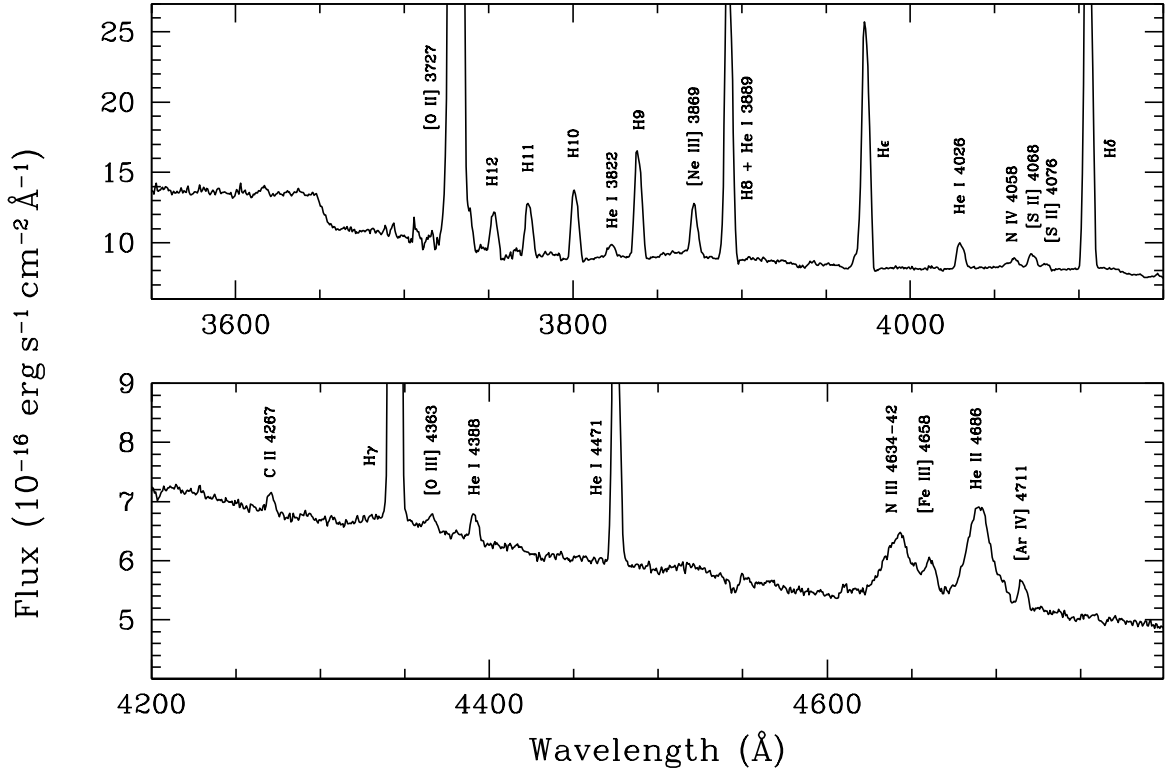


FIG. 3.— Portions of the spectrum of H1013 showing the Balmer discontinuity region and the high-order Balmer lines (top), and the C II λ 4267 recombination line, the [O III] λ 4363 auroral line and the Wolf-Rayet broad emission features around 4650 Å (bottom).

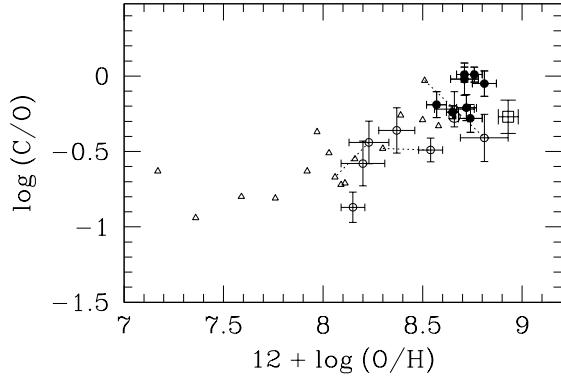


FIG. 4.— C/O ratio as a function of the oxygen abundance O/H from different samples of H II regions. Small triangles represent nebulae in spirals and irregulars for which the abundances have been obtained from collisionally excited lines (Garnett et al. 1995, 1997, 1999; Kobulnicky & Skillman 1998). Recombination line abundances exist instead for the objects represented by open (extragalactic) and solid (Galactic) circles (Esteban et al. 2002, 2005; Peimbert 2003; Peimbert et al. 2005). The dotted lines connect H II regions in common between the two sets. The H1013 H II region is shown as a large open square.

As a first step, the electron temperature from the Balmer jump has been derived. For this purpose, one needs to reproduce the observed Balmer discontinuity, $I(3646^-) - I(3646^+)$, accounting for the continuum processes at work: free-free and free-bound transitions of H I, He I and He II, and two-photon decay of the $2^2S_{1/2}$ level of hydrogen. The corresponding temperature-dependent coefficients have been taken from Brown & Mathews (1970), neglecting the He II contribution, because of the small excitation of H1013, and adopting the He^+/H^+ ratio in Table 5 for the calculation of the He I

contribution. The spectral resolution of the H1013 spectrum is not sufficient to allow a measurement of the real continuum in proximity of the Balmer discontinuity, because the blending of the high-order Balmer lines creates a raised pseudo-continuum. I have therefore extrapolated a fit to the nebular continuum in the $\sim 3800\text{--}3950$ Å wavelength range to the wavelength of the Balmer discontinuity. Using then the ratio of the discontinuity to the H β and H γ emission lines I have derived $T(\text{Bac}) = 5000 \pm 800$ K, where the error is dominated by the extrapolation of the continuum.

In order to derive the average temperature T_0 and the mean square temperature fluctuation t^2 the following equations were used:

$$T[\text{OIII}] = T_0 \left[1 + \left(\frac{91300}{T_0} - 3 \right) \frac{t^2}{2} \right] \quad (7)$$

$$T(\text{Bac}) = T_0(1 - 1.67t^2) \quad (8)$$

yielding $T_0 = 5500 \pm 700$ K, $t^2 = 0.06 \pm 0.02$. Comparable values of t^2 have been found for other extragalactic H II regions. For example, $t^2 = 0.041$ in NGC 5461 and $t^2 = 0.074$ in NGC 5471 (both H II regions located in M101 and studied by Esteban et al. 2002), $t^2 = 0.064\text{--}0.098$ in NGC 2363 (Gonzalez-Delgado et al. 1994), $t^2 = 0.054\text{--}0.076$ in regions X and V of NGC 6822 (Peimbert et al. 2005), $t^2 = 0.033$ in 30 Doradus (Peimbert 2003).

The effect of temperature fluctuations is to increase the chemical abundance measured from collisionally excited lines determined assuming $t^2 = 0$. The ionic abundances in Table 4 were therefore corrected for the case $t^2 \neq 0$, following Peimbert & Costero (1969). The results are summarized in Table 6. As the table shows, the correction to the oxygen

TABLE 6
H1013: IONIC AND TOTAL ABUNDANCES CORRECTED FOR
 $t \neq 0$

	$t^2 = 0.00$	$t^2 = 0.06$
O^+/H^+	$2.3 \pm 0.2 \times 10^{-4}$	$4.7 \pm 0.4 \times 10^{-4}$
O^{++}/H^+	$9.9 \pm 1.4 \times 10^{-5}$	$3.9 \pm 0.6 \times 10^{-4}$
N^+/H^+	$2.6 \pm 0.1 \times 10^{-5}$	$5.1 \pm 0.2 \times 10^{-5}$
S^+/H^+	$1.2 \pm 0.1 \times 10^{-6}$	$2.4 \pm 0.2 \times 10^{-6}$
S^{++}/H^+	$6.7 \pm 0.3 \times 10^{-6}$	$2.9 \pm 0.1 \times 10^{-5}$
Ar^{++}/H^+	$1.3 \pm 0.1 \times 10^{-6}$	$4.1 \pm 0.3 \times 10^{-6}$
Ne^{++}/H^+	$1.1 \pm 0.2 \times 10^{-5}$	$4.7 \pm 0.8 \times 10^{-5}$
$12 + \log(O/H)$	8.52 ± 0.05	8.93 ± 0.05
$\log(N/O)$	-0.95 ± 0.05	-0.96 ± 0.05
$\log(S/O)$	-1.61 ± 0.05	-1.47 ± 0.07

abundance amounts to about 0.4 dex. This upward corrections to O/H is somewhat larger than typically found comparing results from collisionally excited lines and recombination lines. The average correction in a number of H II regions studied in the Milky Way is 0.2 dex (see García-Rojas et al. 2006, Peimbert & Peimbert 2005, and references therein), ranging between 0.11 dex and 0.25 dex. Slightly larger values are found in the extragalactic H II regions NGC 5461 (0.25 dex, Esteban et al. 2002) and Hubble V in NGC 6822 (0.29 dex, Peimbert et al. 2005).

In conclusion, accounting for the presence of temperature fluctuations, the oxygen abundance of H1013 is $12 + \log(O/H) = 8.93 \pm 0.06$. Using the carbon abundance from § 5, the carbon-to-oxygen ratio is $\log(C/O) = -0.27 \pm 0.11$. The measurement of the O II recombination lines in H1013 would improve the accuracy of these determinations, and will require spectroscopic observations at higher spectral resolution than the one used for the current work.

7. DISCUSSION

In this section I consider the results obtained for the inner H II regions of M101 within the context of the calibration of nebular metallicity indicators based on strong lines, in particular R_{23} . In general most of the following considerations could be applied to other strong-line diagnostics, some of which do not suffer some of the problems that affect R_{23} . The major one is the well-known double valuedness of the parameter, that is the fact that a given R_{23} value corresponds to two values of the oxygen abundance. An emission line diagnostic that is monotonically increasing with abundance, such as $[N II]/[O II]$, can be used to remove the degeneracy and place an H II region in the correct branch. For the metal-rich H II regions that are of interest here, only the upper branch calibration is relevant. Secondly, R_{23} is sensitive to the ionization parameter (Pérez-Montero & Díaz 2005). This can be accounted for, in principle, using $[O III]/[O II]$ (McGaugh 1991) or $[O III]/([O III] + [O II])$ (the P index, Pilyugin 2001). Despite these drawbacks, R_{23} is preferentially considered in what follows because of its wide application in the literature, and because much of the recent empirical work deals with this indicator.

7.1. Abundance biases

This work has extended the auroral line method of abundance determination to a fractional galactocentric distance in

M101 of $R/R_0 = 0.10$ (~ 3 kpc) and to an oxygen abundance $12 + \log(O/H) = 8.74$. The innermost H II region studied by KBG03 was H1013 ($R/R_0 = 0.19$). The oxygen abundance they determined from the $[S III]$ and $[N II]$ auroral lines has been revised to a ~ 0.2 dex lower value with the detection of $[O III] \lambda 4363$ in this paper. Both H1013 and the H II region closest to the center analyzed here, H493, have been found to fit the oxygen abundance gradient in M101 quite well. A systematic offset from this gradient would be expected if metal-rich H II regions are affected by strong abundance biases. The result obtained for H493 and H1013 then suggests that the biases due to large-scale temperature fluctuations in H II regions of approximately solar metallicity, $12 + \log(O/H) = 8.7$, are not as large as the maximum value predicted by photoionization models (a ~ 0.2 dex systematic effect in the case of abundances based on $[O III] \lambda 4363$, Stasińska 2005), or that the expected abundance biases become relevant at a somewhat larger metallicity, perhaps around $12 + \log(O/H) = 9.0$. In either case, the abundances obtained from auroral lines in this and in previous papers (e.g. Bresolin et al. 2004) up to approximately the solar metallicity, i.e. what one finds in the very central regions of metal-rich spiral galaxies, appear to be robust (a similar argument is also presented by Pilyugin et al. 2006).

7.2. Metallicity dependent excitation

The direct abundances measured in recent years from auroral-to-nebular line ratios (Castellanos et al. 2002; KBG03, Bresolin et al. 2004, 2005) have provided the necessary input for the empirical calibration of strong-line abundance indicators for metal-rich H II regions. The P -method of Pilyugin (2000, 2001) has been recently recalibrated at high metallicity by Pilyugin & Thuan (2005) on the basis of the recent T_e -based abundances. As mentioned earlier, this empirical calibration leads to H II region abundances that are, in the case of objects located in the metal-rich, upper branch of R_{23} , factors of 2-3 lower than those derived from calibrations based on photoionization models. In order to calibrate indicators that can provide abundances of star-forming galaxies across the universe with accuracies of, say, 0.1 dex, it is crucial to understand the origin of the discrepancies between different calibrations, and try to test them against additional empirical methods. The main difficulty is to provide accurate metallicities for H II regions in the $\log R_{23} < 0.5$ regime, corresponding approximately to $(O/H) > (O/H)_{\odot}$, due to the weakness of the direct abundance diagnostics.

In Pilyugin's method, R_{23} depends not only on the oxygen abundance, but also on a measure of the nebular ionization, parameterized by the excitation parameter $P = [O III] \lambda \lambda 4959, 5007 / ([O III] \lambda \lambda 4959, 5007 + [O II] \lambda 3727)$. This follows the original suggestion by McGaugh (1991) to introduce a two-dimensional characterization of nebular spectra. It is worth pointing out here the empirical finding that the extragalactic H II regions that extend along the upper branch of the R_{23} vs. (O/H) diagram below $\log R_{23} = 0.5$ tend to have a low excitation parameter. In fact, an increase in the metallicity (decreasing R_{23}) corresponds, in a statistical sense, to a decrease in P , i.e. high metallicity H II regions with a measured value of T_e tend to be also low excitation nebulae. This can be seen by plotting R_{23} against O/H , together with curves of constant P (see, for example, Fig. 12 of Pilyugin & Thuan 2005), and can be viewed in light of the

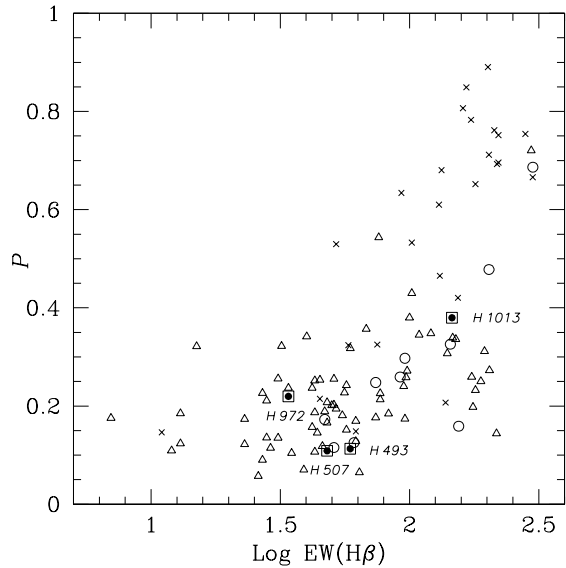


FIG. 5.— Trend of decreasing equivalent width of $H\beta$ with decreasing excitation parameter P . The dots represent H II regions samples in M101 (KBG03, crosses), M51 (Bresolin et al. 2004, open circles), and in five additional spiral galaxies (Bresolin et al. 2005, open triangles). The four M101 H II regions studied in this work are labeled (square-dot symbols).

correlation between galactocentric distance and equivalent width of the $H\beta$ nebular emission line, $EW(H\beta)$, noted in the early abundance studies of spiral galaxies (Searle 1971, Shields & Tinsley 1976). This is shown in Fig. 5, where $\log EW(H\beta)$ is plotted against P for the H II region samples of KBG03, Bresolin et al. (2004, 2005) and for the M101 H II regions studied in this paper. This plot illustrates the fact that the ionizing clusters of H II regions located in the metal-rich inner regions of spiral galaxies are characterized by smaller effective temperatures than those further away from the galactic nuclei (Bresolin & Kennicutt 2002). A metallicity dependence of the ionization parameter $U = Q_{H^0}/4\pi R_S^2 n_c$ (the ratio of ionizing photon density to atom density; R_S is the Strömberg radius), as well as the relatively narrow range in the observed U values, have been noted in studies of extragalactic H II regions several times (e.g. Dopita & Evans 1986; Bresolin et al. 1999; Kewley & Dopita 2002), and have been confirmed by recent investigations of the integrated spectra of star-forming galaxies (Nagao et al. 2006; Maier et al. 2006; Liang et al. 2006). The lower excitation of metal-rich nebulae can be explained by a combination of factors. First of all, stellar atmospheres of massive O stars become cooler with increasing metallicity, as a result of enhanced line and wind blanketing (Massey et al. 2005). Moreover, Dopita et al. (2006b) have shown that the ionization parameter is determined by the ratio of the ionizing photons (a decreasing function of metallicity, due to enhanced stellar atmosphere opacities) to the mechanical energy input from the ionizing O stars (an increasing function of metallicity, since the photon momentum is more efficiently transferred to the stellar wind as the abundance of absorbers increases, Bresolin & Kudritzki 2004). The resulting metallicity dependence derived by Dopita et al., given approximately by $U \propto Z^{-0.8}$, is in good agreement with some empirical measurements. For example, Bresolin et al. (1999) estimated a factor 4 decrease in U varying the metallicity from $0.2 Z_\odot$ to $1.0 Z_\odot$.

7.3. Temperature fluctuations

The analysis based on the classic auroral line method provides lower limits to the oxygen abundance in H II regions. Accounting for the presence of temperature fluctuations leads to higher abundances relative to what is derived by assuming a constant temperature. Temperature fluctuations in nebulae can be estimated in different ways. As done here in the case of H1013, one can compare the temperature derived from the Balmer (or Paschen) continuum with $T[O III]$ (or other ionic temperature measured from an auroral-to-nebular line ratio). In virtually all of the Galactic and extragalactic H II regions with $12 + \log(O/H) \gtrsim 8.1$ in which this comparison has been carried out, the former is found to be significantly lower than the latter (e.g. Peimbert et al. 2000; Peimbert 2003; García-Rojas et al. 2006). For a sample of metal-poor [$12 + \log(O/H) = 7.1-8.3$] emission-line galaxies Guseva et al. (2006) found, instead, that the two temperatures do not differ significantly, while Hägele et al. (2006) found that only one out of three metal-poor [$12 + \log(O/H) = 7.9-8.0$] H II galaxies shows significant temperature fluctuations.

It is also possible to estimate t^2 by requiring that the abundances obtained from collisionally excited lines and from recombination lines match (Peimbert et al. 1993), and from the analysis of helium recombination lines (Peimbert et al. 2000, 2005). These methods have provided consistent results whenever a comparison has been attempted (Esteban et al. 2004; García-Rojas et al. 2004). In extragalactic H II regions of high metal content the most feasible approach is the one adopted here for H1013, since metal recombination lines are difficult to detect. As the excitation of the H II regions decreases with increasing metallicity (Fig. 5), the O II lines become fainter, despite the increase in the oxygen abundance. Even so, further efforts to detect metal recombination lines in high-metallicity nebulae, similar to what has been done for $C II \lambda 4267$ in H1013, would be very valuable. A somewhat higher spectral resolution ($R \sim 5,000-10,000$) than the one used in this work on M101 will aid in the detection of these lines, as well as allow to disentangle lines belonging to a multiplet, such as O II.

The effects of temperature fluctuations on the derivation of nebular abundances need to be accounted for in the calibration of metallicity indicators based on strong lines. In Galactic and extragalactic H II regions an increase in oxygen abundance by a typical factor of 2 to 3 is found relative to the results obtained from collisionally excited lines under the assumption of $t^2 = 0$. Recently, Peimbert et al. (2006) have compiled a list of H II regions where the abundances have been measured, mostly by the same authors, via metal recombination lines, as well as from collisionally excited lines, with the goal of establishing a preliminary calibration of R_{23} as a function of (O/H) from the recombination line technique. Fig. 6 shows the abundances measured in H1013 from this paper, for $t^2 = 0$ (large open square) and for $t^2 = 0.06$ (large full square), in the $12 + \log(O/H)$ vs. $\log R_{23}$ plane. The H II regions in the Peimbert et al. (2006) compilation are shown by the small open squares (abundances from collisionally excited lines, $t^2 = 0$) and by the small filled squares (abundances from metal recombinations lines or from an estimate of t^2 based on the Balmer continuum temperature). All objects plotted in the diagram belong to the upper branch of R_{23} , including those in the comparison sample of metal-rich H II regions from KBG03 and Bresolin et al. (2004, 2005, crosses, open triangles and open circles, respectively). The H II region

H1013 in M101 is currently the extragalactic nebula that lies at the lowest R_{23} value among those that currently have a t^2 estimate. Its oxygen and carbon abundances are among the highest measured so far in this relatively small sample (18 objects).

In Fig. 6 the empirical measurements are compared with the P -method calibration of Pilyugin & Thuan (2005) for two representative values of P (0.2 and 0.6, solid curves). The nebular line-based abundances, derived by neglecting temperature fluctuations (open symbols), are well represented by these curves, and show the tendency mentioned above for a decreasing excitation parameter as the metallicity increases. The abundances derived from metal-recombination lines or accounting for temperature inhomogeneities (solid squares) are displaced upward by about 0.3 dex, approaching the theoretical calculations from photoionization models, taken from Kobulnicky & Kewley (2004) for two different values of the ionization parameter, 10^7 cm s^{-1} and 10^8 cm s^{-1} (these correspond to values of the dimensionless ionization parameter $U = q/c$ of approximately $\log U = -3.5$ and $\log U = -2.5$, respectively). Despite the difficulties that photoionization models have at reproducing emission lines of real nebulae that are very sensitive to T_e , such as [O III] $\lambda 4363$, they are more successful with lines that have a smaller T_e dependence, such as [O II] $\lambda 3727$ and [O III] $\lambda 5007$. This would explain the relatively good agreement found in Fig. 5 with the abundance determinations that account for temperature fluctuations (Peimbert et al. 2006). Still, the problem remains that standard photoionization models predict values for t^2 in H II regions that are very small, between 0.001 and 0.01, compared to observed values between 0.02 and 0.09 (Peimbert 1995; Perez 1997).

In future observations it will be important to extend the sample of objects where the abundances are obtained from recombination lines to lower values of R_{23} , down to $\log R_{23} \sim 0$, if we want to establish a calibration of R_{23} based on recombination lines and/or t^2 determinations that can be used at the highest metallicities. This is made somewhat problematic by the weakness of the metal recombination lines and by the difficulty in obtaining reliable Balmer continuum temperatures. Therefore, it is still valuable to measure nebular abundances from [O III] $\lambda 4363$ and other auroral lines in the high-metallicity regime, since, under the temperature fluctuation paradigm, they appear to provide good estimates for the lower limits in abundance.

7.4. [N II]/[O II]

As mentioned before, the [N II]/[O II] ratio can be used to remove the ambiguity between the lower and upper branches of R_{23} . In fact, Dopita et al. (2000) showed that this ratio is an excellent abundance indicator by itself, superior to R_{23} because of its monotonic dependence on metallicity and its insensitivity to the nebular excitation. In Fig. 7 I show $x = \log([\text{N II}]/[\text{O II}])$ as a function of T_e -based oxygen abundances for the same extragalactic H II regions included in Fig. 6, supplemented at the lower-abundance end by the samples studied by Garnett et al. (1997), van Zee et al. (1998) and van Zee & Haynes (2006) (Pérez-Montero & Díaz 2005 showed a similar plot that includes a larger sample of objects). A simple fit to these data (dashed line) is:

$$12 + \log(\text{O}/\text{H}) = 8.66 + 0.36x - 0.17x^2 \quad (9)$$

According to the models by Dopita et al. (2006a, their Fig. 7),

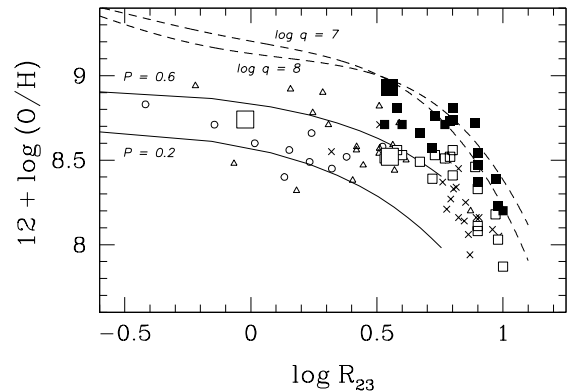


FIG. 6.— The upper, high-metallicity branch of R_{23} . Samples of metal-rich H II regions are taken from KBG03 (crosses) and Bresolin et al. (2004, 2005, open triangles and open circles, respectively). Small squares represent Galactic and extragalactic H II regions, compiled by Peimbert et al. (2006), where abundances have been derived both from collisionally excited lines under the assumption $t^2 = 0$ (open symbols) and from metal recombination lines or an estimate of t^2 (full symbols). The H II regions H493 and H1013 studied in this paper are represented by the large square symbols. The P -method calibration of Pilyugin & Thuan (2005) is shown for $P = 0.2$ and $P = 0.6$ (full lines). The R_{23} calibration based on photoionization models by Kobulnicky & Kewley (2004) is drawn for two values of the ionization parameter, $q = 10^7 \text{ cm s}^{-1}$ ($\log U = -3.5$) and $q = 10^8 \text{ cm s}^{-1}$ ($\log U = -2.5$) (dashed lines).

a given x corresponds with very good approximation to a unique value of the metallicity. The $12 + \log(\text{O}/\text{H})$ values taken from the Dopita et al. models are indicated in the bottom portion of Fig. 7. This helps to illustrate the typical result that abundance diagnostics calibrated via photoionization models provide oxygen abundances about 0.2 dex larger than those obtained from direct methods. From what has been shown in Section 7.3, temperature fluctuations might offer an explanation for this discrepancy. The empirical calibration of the [N II]/[O II] abundance diagnostic also shows that, despite the fact that this line ratio is not sensitive to the ionization parameter, the accuracy of the oxygen abundances that can be derived from it is not better than what can be obtained from R_{23} . The rms of the fit shown in Fig. 7 is 0.20 dex, while limiting the fit to objects that are on the R_{23} upper branch (the extragalactic H II regions shown in Fig. 6) gives $rms \sim 0.15$, the same one obtains by fitting these abundances as a function of $\log R_{23}$. This suggests that our poor knowledge of additional parameters affecting the spectra of H II regions, such as the temperature and ionization structures, currently limits the accuracy in determining abundances from strong-line diagnostics.

8. CONCLUSIONS

In this paper I have presented new deep spectra obtained with Keck/LRIS of four H II regions located in the central, metal-rich (O/H above solar) zone of the spiral galaxy M101. The main results obtained are summarized as following:

- electron temperatures have been measured from auroral-to-nebular line ratios for two H II regions, H493 and H1013. The classic analysis based on collisionally excited lines provides oxygen abundances of $12 + \log(\text{O}/\text{H}) = 8.74 \pm 0.17$ and $12 + \log(\text{O}/\text{H}) = 8.52 \pm 0.05$ for these two objects, respectively. These measurements extend the direct determination of the radial abundance gradient in M101 to about 3 kpc from the

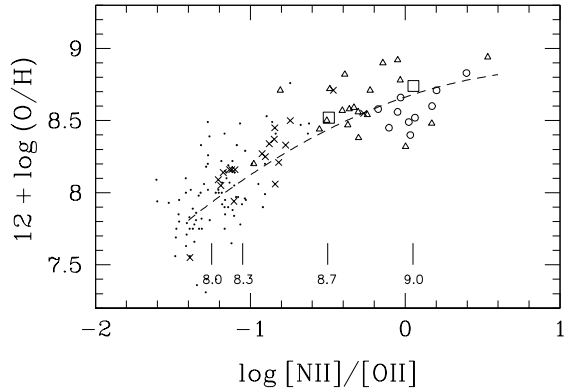


FIG. 7.— Empirical relation between $[\text{N II}] \lambda 6583 / [\text{O II}] \lambda 3727$ and oxygen abundance. The H II regions plotted are the same as in Fig. 6, using the same symbols. The additional low metallicity points (small dots) are from Garnett et al. (1997), van Zee et al. (1998) and van Zee & Haynes (2006). The simple fit to the data given by Eq. 9 is shown as a dashed curve. Four different values of O/H, taken from the models by Dopita et al. (2006a), are indicated at the bottom of the diagram.

center ($R/R_0 = 0.10$).

- the C II $\lambda 4267$ recombination line has been measured in H1013. Accounting for the unseen C^+/H^+ fraction with the aid of photoionization models, a total carbon abundance $12 + \log(\text{C}/\text{H}) = 8.66 \pm 0.07$ (approximately 1.9 times the solar value) is found.

- for H1013 the comparison between the electron temperature derived from the Balmer jump, $T(\text{Bac}) = 5000$ K, and

the electron temperature derived from $[\text{O III}] \lambda 4363 / \lambda 5007$, $T[\text{O III}] = 7700$ K, leads to a mean square temperature fluctuation $t^2 = 0.06 \pm 0.02$, with a volume averaged temperature $T_0 = 5500 \pm 700$ K.

- correcting the abundances derived from the collisionally excited lines for the effect of temperature inhomogeneities increases the oxygen abundance in H1013 by almost 0.4 dex, to $12 + \log(\text{O}/\text{H}) = 8.93 \pm 0.05$. Combining this result with the carbon abundance derived from C II $\lambda 4267$ gives $\log(\text{C}/\text{O}) = -0.27 \pm 0.11$.

- these results indicate that there is still no empirical verification of the strong abundance biases from temperature gradients predicted theoretically for metal-rich H II regions.

- temperature fluctuations can quantitatively explain the current abundance discrepancy of ~ 0.2 - 0.3 dex between empirical indicators and theoretical models.

Future observational work needs to target high-metallicity, low excitation H II regions in the local Universe with medium resolution spectroscopy, in search for metal recombination lines. From these, chemical abundances that are virtually independent of the temperature structure of H II regions can be derived. This would allow more accurate calibrations of strong-line metallicity indicators.

It is a pleasure to thank Manuel Peimbert for encouragement and suggestions.

REFERENCES

- Alloin, D., Collin-Souffrin, S., Joly, M., & Vigroux, L. 1979, *A&A*, 78, 200
- Asplund, M., Grevesse, N., & Sauval, A. J. 2005, in *ASP Conf. Ser. 336: Cosmic Abundances as Records of Stellar Evolution and Nucleosynthesis*, ed. T. G. Barnes, III & F. N. Bash, p. 25
- Asplund, M., Grevesse, N., Sauval, A. J., Allende Prieto, C., & Kiselman, D. 2004, *A&A*, 417, 751
- Benjamin, R. A., Skillman, E. D., & Smits, D. P. 1999, *ApJ*, 514, 307
- Borges Fernandes, M., de Araujo, F. X., Bastos Pereira, C., & Codina Landaberry, S. J. 2001, *ApJS*, 136, 747
- Bresolin, F., Garnett, D. R., & Kennicutt, R. C. 2004, *ApJ*, 615, 228
- Bresolin, F. & Kennicutt, Jr., R. C. 2002, *ApJ*, 572, 838
- Bresolin, F., Kennicutt, Jr., R. C., & Garnett, D. R. 1999, *ApJ*, 510, 104
- Bresolin, F. & Kudritzki, R. P. 2004, in *Origin and Evolution of the Elements*, ed. A. McWilliam & M. Rauch (Cambridge, CUP), 283–296
- Bresolin, F., Schaerer, D., González Delgado, R. M., & Stasińska, G. 2005, *A&A*, 441, 981
- Brown, R. L. & Mathews, W. G. 1970, *ApJ*, 160, 939
- Carigi, L., Peimbert, M., Esteban, C., & García-Rojas, J. 2005, *ApJ*, 623, 213
- Castellanos, M., Díaz, A. I., & Terlevich, E. 2002, *MNRAS*, 329, 315
- Charlot, S. & Longhetti, M. 2001, *MNRAS*, 323, 887
- Chiappini, C., Romano, D., & Matteucci, F. 2003, *MNRAS*, 339, 63
- Davey, A. R., Storey, P. J., & Kisielius, R. 2000, *A&AS*, 142, 85
- Denicoló, G., Terlevich, R., & Terlevich, E. 2002, *MNRAS*, 330, 69
- Díaz, A. I. & Pérez-Montero, E. 2000, *MNRAS*, 312, 130
- Dopita, M. A. & Evans, I. N. 1986, *ApJ*, 307, 431
- Dopita, M. A., Fischera, J., Sutherland, R. S., Kewley, L. J., Leitherer, C., Tuffs, R. J., Popescu, C. C., van Breugel, W., & Groves, B. A. 2006a, *astro-ph/0608062*
- Dopita, M. A., Fischera, J., Sutherland, R. S., Kewley, L. J., Tuffs, R. J., Popescu, C. C., van Breugel, W., Groves, B. A., & Leitherer, C. 2006b, *ApJ*, 647, 244
- Dopita, M. A., Kewley, L. J., Heisler, C. A., & Sutherland, R. S. 2000, *ApJ*, 542, 224
- Edmunds, M. G. & Pagel, B. E. J. 1984, *MNRAS*, 211, 507
- Erb, D. K., Shapley, A. E., Pettini, M., Steidel, C. C., Reddy, N. A., & Adelberger, K. L. 2006, *ApJ*, 644, 813
- Esteban, C., García-Rojas, J., Peimbert, M., Peimbert, A., Ruiz, M. T., Rodríguez, M., & Carigi, L. 2005, *ApJ*, 618, L95
- Esteban, C., Peimbert, M., García-Rojas, J., Ruiz, M. T., Peimbert, A., & Rodríguez, M. 2004, *MNRAS*, 355, 229
- Esteban, C., Peimbert, M., Torres-Peimbert, S., & Rodríguez, M. 2002, *ApJ*, 581, 241
- Ferland, G. J., Korista, K. T., Verner, D. A., Ferguson, J. W., Kingdon, J. B., & Verner, E. M. 1998, *PASP*, 110, 761
- Freedman, W. L., Madore, B. F., Gibson, B. K., Ferrarese, L., Kelson, D. D., Sakai, S., Mould, J. R., Kennicutt, Jr., R. C., Ford, H. C., Graham, J. A., Huchra, J. P., Hughes, S. M. G., Illingworth, G. D., Macri, L. M., & Stetson, P. B. 2001, *ApJ*, 553, 47
- García-Rojas, J., Esteban, C., Peimbert, M., Costado, M. T., Rodríguez, M., Peimbert, A., & Ruiz, M. T. 2006, *MNRAS*, 368, 253
- García-Rojas, J., Esteban, C., Peimbert, M., Rodríguez, M., Ruiz, M. T., & Peimbert, A. 2004, *ApJS*, 153, 501
- Garnett, D. R. 1992, *AJ*, 103, 1330
- Garnett, D. R., Edmunds, M. G., Henry, R. B. C., Pagel, B. E. J., & Skillman, E. D. 2004a, *AJ*, 128, 2772
- Garnett, D. R., Kennicutt, Jr., R. C., & Bresolin, F. 2004b, *ApJ*, 607, L21
- Garnett, D. R., Shields, G. A., Peimbert, M., Torres-Peimbert, S., Skillman, E. D., Dufour, R. J., Terlevich, E., & Terlevich, R. J. 1999, *ApJ*, 513, 168
- Garnett, D. R., Skillman, E. D., Dufour, R. J., Peimbert, M., Torres-Peimbert, S., Terlevich, R., Terlevich, E., & Shields, G. A. 1995, *ApJ*, 443, 64
- Garnett, D. R., Skillman, E. D., Dufour, R. J., & Shields, G. A. 1997, *ApJ*, 481, 174
- Gonzalez-Delgado, R. M., Perez, E., Tenorio-Tagle, G., Vilchez, J. M., Terlevich, E., Terlevich, R., Telles, E., Rodríguez-Espinosa, J. M., Mas-Hesse, M., García-Vargas, M. L., Diaz, A. I., Cepa, J., & Castaneda, H. 1994, *ApJ*, 437, 239
- Guseva, N. G., Izotov, Y. I., & Thuan, T. X. 2006, *ApJ*, 644, 890
- Hadfield, L. J., Crowther, P. A., Schild, H., & Schmutz, W. 2005, *A&A*, 439, 265
- Hägele, G. F., Perez-Montero, E., Diaz, A. I., Terlevich, E., & Terlevich, R. 2006, *MNRAS*, 372, 293
- Hillier, D. J., Crowther, P. A., Najarro, F., & Fullerton, A. W. 1998, *A&A*, 340, 483
- Hodge, P. W., Gurwell, M., Goldader, J. D., & Kennicutt, R. C. 1990, *ApJS*, 73, 661
- Howarth, I. D. 1983, *MNRAS*, 203, 301

- Keenan, F. P., Aller, L. H., Ramsbottom, C. A., Bell, K. L., Crawford, F. L., & Hyung, S. 2000, *Proceedings of the National Academy of Science*, 97, 4551
- Kennicutt, R. C., Bresolin, F., & Garnett, D. R. 2003, *ApJ*, 591, 801
- Kennicutt, R. C. & Garnett, D. R. 1996, *ApJ*, 456, 504
- Kewley, L. J. & Dopita, M. A. 2002, *ApJS*, 142, 35
- Kobulnicky, H. A. & Kewley, L. J. 2004, *ApJ*, 617, 240
- Kobulnicky, H. A. & Skillman, E. D. 1998, *ApJ*, 497, 601
- Krisciunas, K., Sinton, W., Tholen, K., Tokunaga, A., Golisch, W., Griep, D., Kaminski, C., Impey, C., & Christian, C. 1987, *PASP*, 99, 887
- Lamareille, F., Contini, T., Brinchmann, J., Le Borgne, J.-F., Charlot, S., & Richard, J. 2006, *A&A*, 448, 907
- Lee, H., Skillman, E. D., Cannon, J. M., Jackson, D. C., Gehrz, R. D., Polomski, E. F., & Woodward, C. E. 2006, *ApJ*, 647, 970
- Liang, Y. C., Yin, S. Y., Hammer, F., Deng, L. C., Flores, H., & Zhang, B. 2006, *astro-ph/0607074*
- Liu, X.-W., Storey, P. J., Barlow, M. J., Danziger, I. J., Cohen, M., & Bryce, M. 2000, *MNRAS*, 312, 585
- Luridiana, V., Peimbert, M., & Leitherer, C. 1999, *ApJ*, 527, 110
- Maier, C., Lilly, S. J., Carollo, C. M., Meisenheimer, K., Hippelein, H., & Stockton, A. 2006, *ApJ*, 639, 858
- Maier, C., Lilly, S. J., Carollo, C. M., Stockton, A., & Brodwin, M. 2005, *ApJ*, 634, 849
- Massey, P. 2003, *ARA&A*, 41, 15
- Massey, P., Puls, J., Pauldrach, A. W. A., Bresolin, F., Kudritzki, R. P., & Simon, T. 2005, *ApJ*, 627, 477
- McGaugh, S. S. 1991, *ApJ*, 380, 140
- Meynet, G. & Maeder, A. 2005, *A&A*, 429, 581
- Mouchine, M., Bamford, S. P., Aragón-Salamanca, A., Nakamura, O., & Milvang-Jensen, B. 2006, *MNRAS*, 369, 891
- Nagao, T., Maiolino, R., & Marconi, A. 2006, *astro-ph/0603580*
- Oke, J. B., Cohen, J. G., Carr, M., Cromer, J., Dingizian, A., Harris, F. H., Labrecque, S., Lucinio, R., Schaal, W., Epps, H., & Miller, J. 1995, *PASP*, 107, 375
- Pagel, B. E. J., Edmunds, M. G., Blackwell, D. E., Chun, M. S., & Smith, G. 1979, *MNRAS*, 189, 95
- Peimbert, A. 2003, *ApJ*, 584, 735
- Peimbert, A. & Peimbert, M. 2005, in *Revista Mexicana de Astronomia y Astrofisica Conference Series*, 9–14
- Peimbert, A., Peimbert, M., & Ruiz, M. T. 2005, *ApJ*, 634, 1056
- Peimbert, M. 1967, *ApJ*, 150, 825
- Peimbert, M. 1995, in *The Analysis of Emission Lines*, ed. R. Williams & M. Livio, p. 165
- Peimbert, M. & Costero, R. 1969, *Boletín de los Observatorios Tonantzintla y Tacubaya*, 5, 3
- Peimbert, M. & Peimbert, A. 2006, *RMxAC*, 26, 163
- Peimbert, M., Peimbert, A., Esteban, C., Garcia-Rojas, J., Bresolin, F., Carigi, L., Ruiz, M. T., & Lopez-Sanchez, A. R. 2006, *astro-ph/0608440*
- Peimbert, M., Peimbert, A., & Ruiz, M. T. 2000, *ApJ*, 541, 688
- Peimbert, M., Peimbert, A., Ruiz, M. T., & Esteban, C. 2004, *ApJS*, 150, 431
- Peimbert, M., Storey, P. J., & Torres-Peimbert, S. 1993, *ApJ*, 414, 626
- Perez, E. 1997, *MNRAS*, 290, 465
- Pérez-Montero, E. & Díaz, A. I. 2005, *MNRAS*, 361, 1063
- Pettini, M. & Pagel, B. E. J. 2004, *MNRAS*, 348, L59
- Pilyugin, L. S. 2000, *A&A*, 362, 325
- , 2001, *A&A*, 369, 594
- Pilyugin, L. S. & Thuan, T. X. 2005, *ApJ*, 631, 231
- Pilyugin, L. S., Thuan, T. X., & Vílchez, J. M. 2006, *MNRAS*, 367, 1139
- Pilyugin, L. S., Vílchez, J. M., & Contini, T. 2004, *A&A*, 425, 849
- Sakai, S., Ferrarese, L., Kennicutt, R. C., & Saha, A. 2004, *ApJ*, 608, 42
- Salzer, J. J., Lee, J. C., Melbourne, J., Hinz, J. L., Alonso-Herrero, A., & Jangren, A. 2005, *ApJ*, 624, 661
- Savaglio, S., Glazebrook, K., Le Borgne, D., Juneau, S., Abraham, R. G., Chen, H.-W., Crampton, D., McCarthy, P. J., Carlberg, R. G., Marzke, R. O., Roth, K., Jørgensen, I., & Murowinski, R. 2005, *ApJ*, 635, 260
- Searle, L. 1971, *ApJ*, 168, 327
- Seaton, M. J. 1979, *MNRAS*, 187, 73P
- Shapley, A. E., Erb, D. K., Pettini, M., Steidel, C. C., & Adelberger, K. L. 2004, *ApJ*, 612, 108
- Shaw, R. A. & Dufour, R. J. 1995, *PASP*, 107, 896
- Shi, F., Kong, X., & Cheng, F. Z. 2006, *A&A*, 453, 487
- Shields, G. A. & Tinsley, B. M. 1976, *ApJ*, 203, 66
- Stasińska, G. 1978, *A&A*, 66, 257
- , 1980, *A&A*, 85, 359
- , 1982, *A&AS*, 48, 299
- , 2005, *A&A*, 434, 507
- Stasińska, G. 2006, *A&A*, 454, L127
- Stasińska, G. & Schaerer, D. 1999, *A&A*, 351, 72
- Storchi-Bergmann, T., Calzetti, D., & Kinney, A. L. 1994, *ApJ*, 429, 572
- Storey, P. J. & Hummer, D. G. 1995, *MNRAS*, 272, 41
- Tayal, S. S. & Gupta, G. P. 1999, *ApJ*, 526, 544
- Torres-Peimbert, S., Peimbert, M., & Daltabuit, E. 1980, *ApJ*, 238, 133
- Torres-Peimbert, S., Peimbert, M., & Fierro, J. 1989, *ApJ*, 345, 186
- Tremonti, C. A., Heckman, T. M., Kauffmann, G., Brinchmann, J., Charlot, S., White, S. D. M., Seibert, M., Peng, E. W., Schlegel, D. J., Uomoto, A., Fukugita, M., & Brinkmann, J. 2004, *ApJ*, 613, 898
- Tsamis, Y. G. & Péquignot, D. 2005, *MNRAS*, 364, 687
- van Zee, L. & Haynes, M. P. 2006, *ApJ*, 636, 214
- van Zee, L., Salzer, J. J., Haynes, M. P., O'Donoghue, A. A., & Balonek, T. J. 1998, *AJ*, 116, 2805
- Vílchez, J. M. & Esteban, C. 1996, *MNRAS*, 280, 720
- Walborn, N. R. & Fitzpatrick, E. L. 2000, *PASP*, 112, 50
- Zaritsky, D., Kennicutt, Jr., R. C., & Huchra, J. P. 1994, *ApJ*, 420, 87